Analysis of Electron Transfer Properties of ZnO and TiO_2 Photoanodes for Dye-Sensitized Solar Cells

Aravind Kumar Chandiran, Mojtaba Abdi-Jalebi, Mohammad K. Nazeeruddin,* and Michael Grätzel*

Laboratory of Photonics and Interfaces, Swiss Federal Institute of Technology (EPFL), Station 6, Lausanne, CH 1015, Switzerland

ABSTRACT Mesoporous TiO_2 nanoparticle films are used as photoanodes for high-efficiency dye-sensitized solar cells (DSCs). In spite of excellent photovoltaic power conversion efficiencies (PCEs) displayed by titanium dioxide nanoparticle structures, the transport rate of electrons is known to be low due to low electron mobility. So the alternate oxides, including ZnO, that possesses high electron mobility are being investigated as potential candidates for photoanodes. However, the PCE with ZnO is still lower than with TiO_2, and this is typically attributed to the low internal surface area. In this work, we attempt to make a one-to-one comparison of the photovoltaic performance and the electron transfer dynamics involved in DSCs, with ZnO and TiO_2 as photoanodes. Previously such comparative investigations were hampered due to the morphological differences (internal surface area, pore diameter, porosity) that exist between zinc oxide and titanium dioxide films. We circumvent this issue by depositing different thicknesses of these oxides, by atomic layer deposition (ALD), on an arbitrary mesoporous insulating template and subsequently using them as photoanodes. Our results reveal that at an optimal thickness ZnO exhibits photovoltaic performances similar to TiO_2, but the internal electron transfer properties differ. The higher photogenerated electron transport rate contributed to the performances of ZnO, but in the case of TiO_2, it is the low recombination rate, higher dye loading, and fast electron injection.

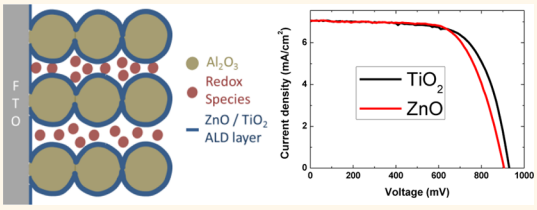

KEYWORDS: dye-sensitized solar cell · zinc oxide · titanium dioxide · atomic layer deposition · nanostructures · cobalt complexes · photovoltaic

Molecular photovoltaics based on dye sensitization offer a unique possibility to tune separately the light-absorbing chromophores and the charge-transporting layers unlike conventional p−n junction device.[1−3] This has led to an explosion in dye sensitizers research and resulted in the development of panchromatic sensitizers, which absorb the entire visible solar spectrum, giving photovoltaic power conversion efficiencies well above 12%.[4] The electron transport layer, typically a mesoporous oxide layer, supports the dye molecules and possesses favorable energetics to accept the photogenerated electrons from the excited state of the dye. An ideal electron transport layer should (1) possess high surface area to enhance dye loading for effective light harvesting, (2) be transparent to visible light to avoid photon loss to the substrate, (3) possess a conduction band sufficiently below the lowest unoccupied molecular orbitals (LUMOs) of the sensitizer to allow near-unity photogenerated electron injection, (4) have high electron mobility for efficient electron transport, (5) be inert to the redox electrolyte to reduce electron recombination rate (k_{rec}, the rate of electron recombination from the photoanode film to the redox mediator), and (6) possess defects or hydroxyl groups to chemisorb dye molecules onto its surface.[3,5−9] Other economic and environmental considerations include material abundance, ease of preparation, and chemical nontoxicity. Conventional oxides including TiO_2,[6,9−15] ZnO,[13,16−31] SnO_2,[9,32,33] and Nb_2O_5[34−39] have been widely explored as electron transport layer in dye-sensitized solar cells (DSCs). Recently, some ternary oxides including $SrTiO_3$,[40−42] $BaSnO_3$,[43] and Zn_2SnO_4[44] also have been studied. Despite tremendous research efforts, nanoparticle anatase TiO_2 still remains the material of choice for DSCs, due to its favorable aforementioned properties coupled with the well-established low-cost synthetic preparation methods in both academic laboratories and industries. The best DSCs with over 12% photovoltaic power conversion

* Address correspondence to mdkhaja.nazeeruddin@epfl.ch, michael.graetzel@epfl.ch.

Received for review October 23, 2013 and accepted February 19, 2014.

Published online February 19, 2014
10.1021/nn405535j

efficiency involve TiO_2 mesoporous nanoparticles of 20 nm with internal surface area of *ca.* 75 m^2/g.[4] In spite of its versatility, the mobility of electrons in TiO_2 is low (0.1−4 $cm^2\ V\ s^{-1}$),[23] and it affects the electron transport rate (k_{trans}, the rate at which the photogenerated electrons are transported from the photoanode film to the external contact) in the photoanode film, leading to a decrease in the collection efficiency ($\eta_{coll} = k_{trans}/(k_{trans} + k_{rec})$) of the photogenerated electrons.[2] ZnO is a well-known material that exhibits electron mobility of *ca.* 200−300 $cm^2\ V\ s^{-1}$ for bulk material and ∼1000 $cm^2\ V\ s^{-1}$ for single-crystal nanowires.[45−47] The mobility of ZnO is orders of magnitude higher than TiO_2, and it manifests the importance of ZnO as a potential candidate for a DSC. The material, so far, has been successfully exploited as a photoanode in the form of nanowires, nanoparticles, nanotubes, nanotips, nanoforests, nanoflowers, nanosheets, nanobelts, or dendrites.[23] Even though literature reports often mention the high electron mobility of ZnO as a major reason for replacing TiO_2, to the best of our knowledge, no one-to-one comparison has been made on the electron transfer properties to show that ZnO is a better photoanode for dye-sensitized solar cells. A comparison of ZnO and TiO_2 photoanodes, which possess different morphological properties or particle sizes, may not give a credible description of the transport properties. On the other hand, to understand the catalytic property for the recombination of electrons from the conduction band of ZnO and TiO_2 material to the electrolyte, any variation in the charge transfer to redox species due to the difference in the internal surface area should be avoided. Similarly, any variation in the porosity or pore diameter in the mesoporous films can result in a difference in the concentration of redox components residing within the pores. Altogether, for a given exchange current density, it may create a difference in the redox shuttle transport within the photoanode film, especially while employing bulky cobalt redox mediators.[4,48,49] So for a legitimate study, both ZnO and TiO_2 mesoporous films should possess similar particle size, internal surface area, pore diameter, porosity, and film thickness, and this is an experimentally challenging task. To realize this goal, we used a 3 μm mesoporous alumina film as an insulating template, onto which different thicknesses of TiO_2 or ZnO are deposited by atomic layer deposition (ALD) (Figure 1).[11,50,51] ALD oxides take the preform of the insulating template, and for any given thickness, the morphological properties are expected to be alike. The ALD technique is selected for deposition of TiO_2 and ZnO, as it is capable of depositing conformal films on any high-aspect-ratio mesoporous structures, unlike other physical or chemical vapor depositions.[52−54] Dye-sensitized solar cells are made using our standard organic donor−π-acceptor dye and cobalt(bipyridine)$_3$ redox electrolyte.[55] The electron transfer properties such as excited state electron injection from the dye, carrier recombination, and transport are investigated in detail. An elaborate comparison of these properties is made at an optimized thickness of 5 nm TiO_2 or ZnO on an alumina template, where a best performance is shown by both the oxides. In this one-to-one comparative study, we show that the electron transport is relatively fast in ZnO compared to the TiO_2 film. However, on other hand, the unwanted recombination rate is also higher for the former, which decreases the attainable open-circuit potential of the device.

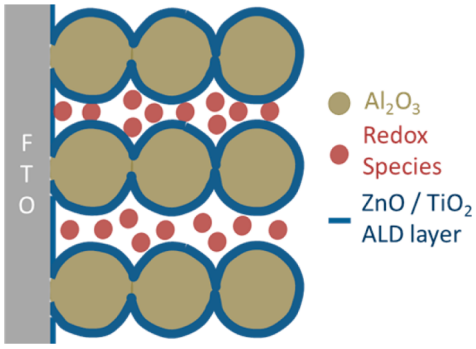

Figure 1. Block diagram of the photoanode. Screen-printed mesoporous alumina nanoparticles (green) are coated with different thicknesses of ZnO or TiO_2 overlayer (blue) by atomic layer deposition techniques. The brown dots represent the redox species in the electrolyte.

RESULTS AND DISCUSSION

The crystallinity of the sintered ALD ZnO on alumina is analyzed using X-ray diffraction techniques, and the collected diffractograms are presented in Figure S1. All the samples from the 3 to 10 nm ZnO overlayer exhibit Bragg reflections corresponding to wurtzite phase (space group: $P6_3mc$, JCPDS card no. 36-1451), confirming the crystallinity of the deposited ALD layers. The broad peak at low 2-theta angles arises from the amorphous nature of the underlying alumina template. Additionally, one has to note that thicker ALD ZnO layers show sharp peaks compared to thinner ones, and it could be attributed to be decreasing crystallinity of the later. The full width at half-maximum for the peaks between 30° and 40° are broader for the thinner ZnO, which is ascribed to the small crystallites. Previously, we have shown that TiO_2 starts to crystallize only at a critical thickness of 5 nm, unlike ZnO, where crystallinity could be already noticed with 3 nm.[11]

These ALD ZnO or TiO_2 layers of different thickness were sensitized with a standard organic donor−π-acceptor dye sensitizer (Y123), and solar cells are made using cobalt(bipyridine)$_3$ electrolyte and a carbon counter electrode.[2] The current−voltage characteristics of the corresponding devices are investigated under AM1.5G solar irradiance (100 mW/cm^2). With a 2 nm ZnO overlayer on a 3 μm alumina template, the device could transport a current density (J_{SC}) of

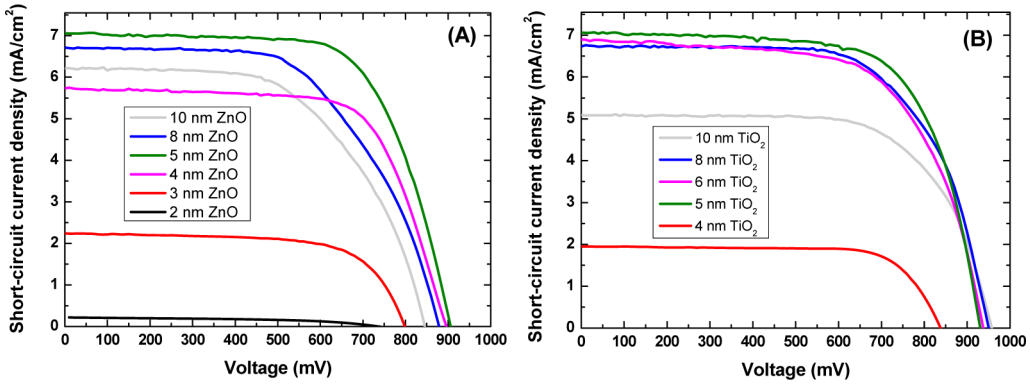

Figure 2. Current−voltage (J−V) curves of dye-sensitized solar cells, measured under AM1.5G solar irradiance (100 mW/cm^2), possessing different thicknesses of either (A) ZnO or (B) TiO_2 ALD overlayer on 3 μm mesoporous alumina templates.

0.22 mA/cm^2, and with an open-circuit potential (V_{OC}) and fill factor (ff), respectively, of 725 mV and 50%, a very low power conversion efficiency (PCE) of 0.08% is attained. On increasing the thickness of ZnO, J_{SC} progressively increases to a maximum of 7.2 mA/cm^2 at 5 nm, and together with an increase of V_{OC} and ff, a PCE of 4.4% is obtained. Further increase in the thickness results in a drop of all the photovoltaic parameters. Similarly, in the case of TiO_2, high power conversion efficiency (4.4%) is obtained with a 5 nm overlayer on the insulating template. Unlike ZnO, increasing the thickness of TiO_2 beyond 6 nm reduced only the current density and not the open-circuit potential or the fill factor of the device. All the photovoltaic curves and parameters are presented in Figure 2, Table 1, and Table 2. To understand the origin of photovoltaic characteristics, a complete investigation is done by analyzing the dye loading, electron injection, recombination, and transport properties.

The absorption spectra of the Y123 dye sensitized on mesoporous Al_2O_3 films containing different thicknesses of TiO_2 and ZnO are presented in Figure 3. Two distinct features can be noted from the spectra; one is the difference in the maximum absorption intensity (A_{max}), and other is the wavelength (λ_{max}) at which the A_{max} occurs. In the case of TiO_2, A_{max} increases when the thickness of the ALD layer is increased from 2 nm to 5 nm. A further increase in the thickness lowered the apparent dye loading (proportional to A_{max}). In addition, λ_{max} shifts drastically to the blue from 481 nm (2 nm TiO_2) to 451 nm (10 nm TiO_2). The shift in λ_{max} is quite dramatic during the first few nanometers of deposition; however, beyond 5 nm TiO_2, λ_{max} shifts by only 7 nm. On the other hand, the deposition of ZnO progressively lowered the dye loading, and unlike titania, λ_{max} did not vary significantly. The variation in λ_{max} can be purely attributed to the modification of the surface pH of the deposited ALD oxides. The significant variation in the λ_{max} on the surface of TiO_2 implies that the dye is more basic (or dye is completely deprotonated) on a 10 nm TiO_2 compared to 2 nm TiO_2. In other words, we can say

TABLE 1. Photovoltaic Parameters of DSCs Made with Different Thicknesses of a ZnO ALD Overlayer on 3 μm Mesoporous Alumina Films, Measured under AM1.5G Solar Irradiance (100 mW/cm^2)

thickness of ZnO (nm)	J_{SC} (mA/cm^2)	V_{OC} (mV)	fill factor (%)	efficiency (%)
2	0.22	725.6	49.6	0.08
3	2.3	798.0	67.0	1.2
4	5.9	896.4	68.8	3.6
5	7.2	905.9	67.2	4.4
8	6.8	878.8	58.2	3.5
10	6.3	845.2	57.3	3.1

TABLE 2. Photovoltaic Parameters of DSCs Made with Different Thicknesses of a TiO_2 ALD Overlayer on 3 μm Mesoporous Alumina Films, Measured under AM1.5G Solar Irradiance (100 mW/cm^2)

thickness of TiO_2 (nm)	J_{SC} (mA/cm^2)	V_{OC} (mV)	fill factor (%)	efficiency (%)
4	1.9	837.5	74.3	1.2
5	7.0	930.2	68.2	4.4
6	6.9	937.2	63.7	4.1
8	6.7	950.3	65.3	4.2
10	5.0	957.5	66.9	3.2

that thicker titania layers are more basic than the thinner ones. In order to prove that the absorption shift to blue (for thicker TiO_2 layers) resulted from the basic nature of the surface, we performed similar absorption studies on the Y123-sensitized mesoporous nanoparticle (np) films of TiO_2, synthesized under acidic and basic medium, and Al_2O_3 (Figure S2). It is well known that alumina surface is more basic compared to the surface of titania.[56] The absorption maximum of the sensitized Y123 dye shows a blue shift on the surface of Al_2O_3 compared to the acidic TiO_2. The titanium dioxide synthesized under alkaline medium exhibits a λ_{max} between these two films. The observed trend in the latter study is similar to the blue shift evidenced in Figure 3B, when increasing the thickness of the ALD TiO_2 overlayer from 2 nm to 10 nm. The difference in the surface property of different thicknesses of ALD TiO_2 overlayers probably arises from the

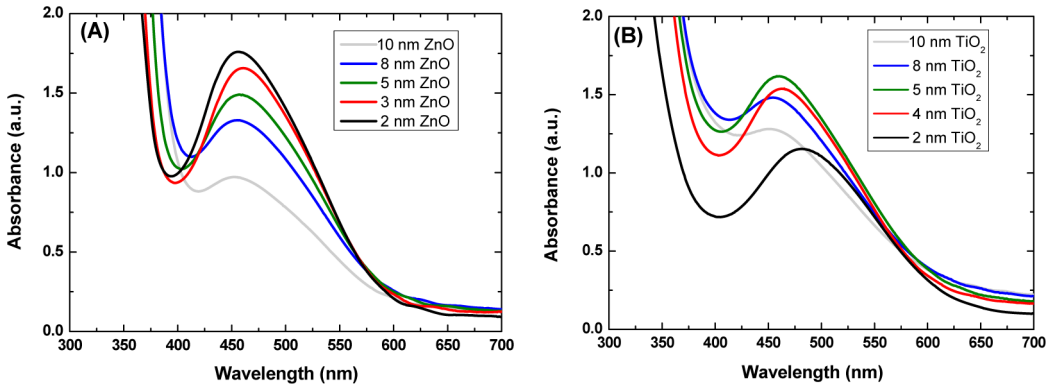

Figure 3. Absorption spectra Y123 dye sensitizer chemisorbed on the surface of different thicknesses of (A) ZnO or (B) TiO_2 on mesoporous Al_2O_3 films.

underlying alumina template. Since ZnO, which is a basic oxide, is grown on the surface of basic alumina, the surface properties of films of different thicknesses are little affected.

The initial increase in the dye uptake (up to 5 nm TiO_2) can be attributed to increasing the basic nature of the surface, but beyond 5 nm the decrease in the surface area, as shown previously,[11,50] dominates the basic properties, and hence a decline is observed. The evolution of absorption observed for ZnO can be ascribed mainly to the decreasing surface area, while the modification in the surface acid-based property might have played a minor role. For a given ALD layer thickness, the amount of dye absorbed on the surface of titanium dioxide is higher compared to ZnO. Figure S3 shows a comparison of absorption spectra of 5 and 10 nm TiO_2/ZnO.

The excited electron injection properties are investigated using time-resolved single photon counting as proposed by Koops *et al.*, by monitoring the excited state emission decay of the adsorbed dye (Figure 4).[57,58] The decay of the excited state is slightly delayed with increasing thickness of titanium dioxide, and it implies a reduction in the injection yield, which increases the probability of radiative decay to the ground state. This could be due to the variation in the pH of the adsorbed dye. However, in the case of ZnO, the excited state exhibits slow decay for a 2 nm overlayer thickness, and a further increase in the thickness enhanced the injection. For thicker overlayers (10 nm), the emission decay is similar for ZnO and TiO_2, and it is due to similar injection properties. The delay in the injection for a thinner ZnO layer could be attributed to the quantum confinement effect, where the bottom of the conduction band is moved toward the vacuum,[59] and also partly to the pH of adsorbed dye molecules.[60]

In order to further understand the difference in the electron injection properties, we probed the density of trap states (DOS) below the conduction band of titanium dioxide or zinc oxide (in a complete device) using charge extraction measurements (Figure S4, Figure S5).

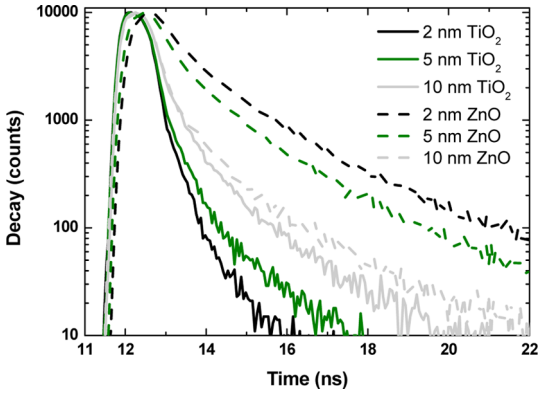

Figure 4. Excited state electron radiative decay of Y123 dye sensitizer on different thicknesses of ZnO and TiO_2 overlayers on mesoporous insulating templates.

For a 5 nm thickness of overlayer, ZnO possesses a shallow DOS distribution (or a negative shift with respect to NHE) compared to TiO_2. The probable reason for the observed negative shift of the conduction band is the quantum confinement effect displayed by the thinner ZnO. It has been previously shown that titanium dioxide can exhibit quantum confinement for particles only less than 3 nm, whereas for ZnO the upper limit is shown to be 5 nm.[59,61] Hence, the overpotential (difference between the energy level of the LUMO of the dye and the bottom of the conduction band of the oxide photoanode) available for the electron injection from the excited state of dye to 5 nm ZnO is lower, leading to a decrease in the injection probability. However, 10 nm overlayers of both ZnO and TiO_2 exhibited similar DOS profiles, and the expected difference between the excited state of the dye and the bottom of the conduction bands in the films (for a given recombination rate and charge density) is similar, displaying similar overpotential for electron injection. These results are consistent with the observation of emission decay.

The electron transport and recombination properties are investigated on the complete photovoltaic devices. Figure 5 shows the transport rate of electrons for different thicknesses of TiO_2 and ZnO overlayer on alumina. At any given voltage, for a 5 nm thick

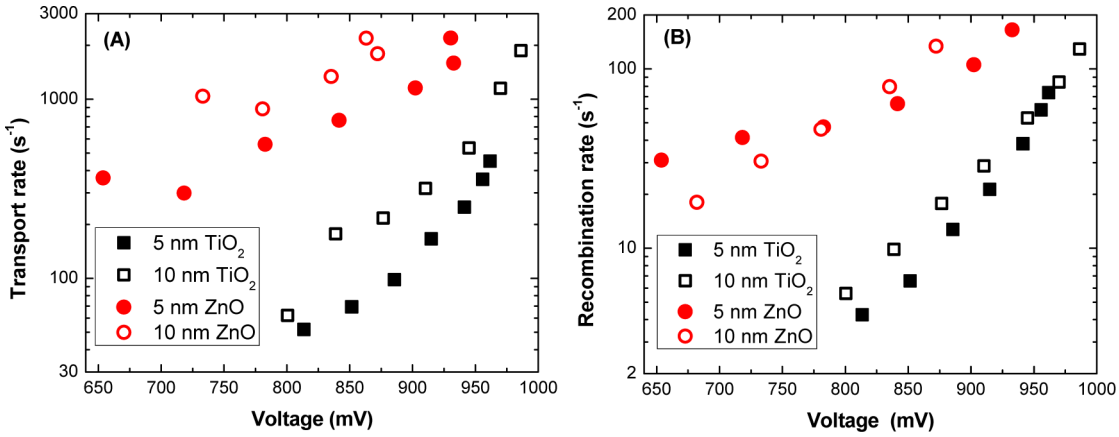

Figure 5. (A) Transport rate and (B) recombination rate of electrons measured using transient decay measurements for a 5 and 10 nm thick ALD overlayer of ZnO or TiO_2.

overlayer (which shows the best photovoltaic efficiency in both the oxides), the electrons are transported by almost an order of magnitude faster in ZnO compared to TiO_2, and this could be attributed to the higher electron mobility in ZnO. However in a previous work by Hagfeldt *et al.*, the electron transport is found to be similar to TiO_2, and yet in another work the trend is found to be opposite; that is, titanium dioxide transports electrons faster than ZnO.[13,21] As stated previously in the introduction, we attribute these ambiguities to the film preparation methods, where the interface connections probably are poor. However in the present case, we solved the problem by making a conformal three-dimensional structure where no particle interface exists but only the crystallite interfaces. When the thickness of the overlayer is increased to 10 nm, the transport rate is slightly enhanced in both the ZnO and TiO_2 overlayer films. This result is consistent with our previous work where we have shown that the transport rate reached a maximum at around a 6 nm thick overlayer of TiO_2.[11] The transport rate plot is also displayed in terms of diffusion coefficient of electrons, in Figure S6.

In spite of possessing favorable transport properties, ZnO, on the other hand, shows very high electron back reaction. That is, the rate of recombination of electrons from the conduction band of ZnO to the oxidized form of the redox species is much higher compared to the titanium dioxide.

DISCUSSION

The current density, which is a function of light harvesting, injection, regeneration, and collection efficiency, shows a steady increase up to 5 nm ZnO/TiO_2, and a drop is observed on increasing the thickness further. Dye regeneration should not be affected, as the dye and electrolyte used in the study are similar, and hence the variation in the current density due to this parameter can be ignored. The injection of excited electrons from the LUMO of the dye to the 5 nm ZnO is slower compared to the TiO_2, and hence for a given amount of photons absorbed, the number of electrons injected into the conduction band of ZnO is lower. For the photoanode films with less than 5 nm ZnO or TiO_2, the current density is predominantly determined by the injection efficiency and the transport rate of injected electrons in the wide band-gap semiconductor film. However, beyond 5 nm, despite a higher transport rate, J_{SC} is governed by the dye uptake on the surface of the mesoporous film. As the dye loading is reduced due to the reduction in the available surface area, a drop in J_{SC} is observed. We cannot exclude the shift of dye $\pi-\pi^*$ maximum observed for the different thicknesses of the oxide overlayers. However, for the best performing 5 nm thick ZnO or TiO_2, the maximum of absorption lies at 457−458 nm, and hence any change in the current density due to the absorption shift can be excluded. The normalized incident photon-to-electron conversion efficiency spectra shown in Figure S7 show a similar onset for both the 5 nm TiO_2 and ZnO, and this result is consistent with the absorption spectra. One has to note that, in spite of a reduction in dye loading and low injection efficiency, ZnO transports 7.2 mA/cm^2, roughly equal to the J_{SC} displayed by TiO_2, for the same thickness. This is attributed to better collection efficiency of the device resulting from higher transport rate. The observed V_{OC} is in general higher for TiO_2-based devices compared to ZnO and is primarily due to the high recombination rate of the photogenerated electrons to the electrolyte in the latter case.

Most of the previous work of ZnO films employed tens of micrometer thick films to achieve similar efficiencies, and this is purely attributed to the low surface area available for dye loading on the synthesized nanostructures. In a recent work on 12 μm thick ZnO nanowires, a dye similar to Y123 yielded only 1.5% PCE.[16] However, in this work, as we use a mesoporous nanoparticle template, the surface area (equivalent to the conventional TiO_2 nanoparticle films) is preserved,

and at the same time, a high mobility three-dimensional conformal ZnO structure is utilized, which leads to 4.4% PCE. Future work incorporates a similar deposition strategy of ZnO on the thicker mesoporous insulating templates for high-efficiency solar cells.

CONCLUSION

In this work, we made a one-to-one comparison on the performance of ZnO and TiO_2 photoanodes for dye-sensitized solar cells. Different thicknesses of zinc oxide and titanium dioxide were deposited by ALD on mesoporous insulating alumina preforms, which act as templates. The best performance is achieved with 5 nm ZnO or TiO_2 overlayer films, where a photovoltaic power conversion efficiency of 4.4% is achieved. An in-depth investigation reveals that the similar photovoltaic performances did not come from similarity in properties but from compensating ones. The transport rate of electrons is faster in ZnO compared to TiO_2, whereas the recombination rate on other hand is also higher. This work shows ZnO is clearly favorable for the systems demanding faster electron transport; however, precaution has be to taken to use inert multielectron slow redox systems, unlike cobalt redox mediators or the spiro-OMetad hole conductor. Future works to decrease catalytic activity of the electron back reaction can include ALD surface treatment by insulating oxides.[60,62,63] Titanium dioxide on the other hand is advantageous in terms of electron recombination, as it is relatively inert to single-electron redox mediators. Also, this is the first time we show 4.4% efficiency on a 3 μm mesoporous film using an ultrathin ZnO overlayer.

METHODS

Photoanode Preparation. A screen-printable alumina paste is made by mixing a commercially available Al_2O_3 nanoparticle with ethyl cellulose of two different viscosities (5−15 mPas, 30−50 mPas, Aldrich) and terpineol (Aldrich) following the procedure described elsewhere.[11] The paste is screen printed on a precleaned transparent conducting glass (NSG10, 10 Ω□ Japan), and the films are dried at 125 °C for 7 min. It is followed by a series of thermal sintering steps (325 °C for 5 min with 15 min ramp time, 375 °C for 5 min with 5 min ramp time, 450 °C for 15 min with 5 min ramp time, and 500 °C for 15 min with 5 min ramp time) to remove the binders and organic residues.[6] The thickness of the screen-printed film is measured using a KLA Tencor alpha-step 500 profiler. The resultant film thickness is 2.8 ± 0.1 μm. The film and mesoporous and nitrogen gas sorption analysis (Micrometrics ASAP2000) gives an average particle size, porosity, and pore diameter of 23 nm, 76%, and 47 nm, respectively. These mesoporous films are used as such for the deposition of either ZnO or TiO_2 by atomic layer deposition.[64−66] ZnO is deposited at a temperature of 150 °C from diethyl zinc (25 °C) (ABCR, Germany) and deionized water (18 MΩ, 25 °C) precursors using a Savannah 100 instrument purchased from Cambridge Nanotech, USA. The precursor vapors are pulsed into the reactor using an inert carrier gas (N_2, 99.999%). The metal precursor is pulsed for 0.02 s and is confined in the reactor for 30 s followed by a purge for 30 s to remove the excess precursor molecules and byproducts of the ALD reaction. It is then followed by the water pulse for 0.015 s and is also confined in the reactor for 30 s with a 30 s purge similar to the metal precursor. The deposition of TiO_2 is achieved by pulsing tetrakis(dimethylamido)titanium(IV) precursor (0.1 s, 75 °C) and H_2O (0.015 s, 25 °C) precursor in two different stages with an inert gas purge in between. Similar to the ZnO deposition, the precursors' pulse and purge times were maintained at 30 s.[11] The growth rate of the films on the Si wafer is measured using spectroscopic ellipsometry (SOPRA GES 5E) over the range of photon energies (1.5 to 5.5 eV), and the obtained data are fitted using WinEli software. Approximately, 5 and 15 cycles of deposition, respectively, contribute to 1 nm growth of ZnO and TiO_2, which is consistent with the literature.

Time-Resolved Single-Photon Counting. Electron injection dynamics was studied on the Y123-sensitized mesoporous films using time-resolved single-photon counting (TRSPC) with Horiba Jobin Yvon Fluorolog-3 spectrofluorometer (Japan) equipped with a NANOLed 406 nm pulsed diode light source with a pulse width of less than 200 ps and repetition rate of 1 MHz. The emission decay is monitored at a wavelength of 625 nm. A 595 nm band-pass filter was used to exclude stray photons reaching the detector that can result from scattering.[57,58]

Device Fabrication. Prior to dipping, the ZnO and TiO_2 films deposited on the Al_2O_3 were fired at 500 °C for 30 min to remove the surface contaminants, and the films are sensitized in a 0.1 mM Y123 solution (3-{6-{4-[bis(2′,4′-dihexyloxybiphenyl-4-yl)amino]phenyl}-4,4-dihexylcyclopenta[2,1-*b*:3,4-*b*′]dithiphene-2-yl}-2-cyanoacrylic acid) in a 50/50 (v/v) acetonitrile/*tert*-butanol mixture for 8 h.[67] The sensitized electrodes were then washed in acetonitrile to remove the loosely bound dye molecules before the cell assembly. The counter electrode was made by drop casting carbon (ABCR, Germany) from an acetone solution on the FTO glass (TEC7, Solaronix, Switzerland). The two electrodes were melt sealed using a 25 μm thick Surlyn (Dupont, USA) polymer film. The electrolyte used was a mixture of 200 mM Co^{2+}, 50 mM Co^{3+}, 100 mM LiTFSI, and 200 mM *tert*-butylpyridine in acetonitrile solvent. This electrolyte was injected by a vacuum backfilling technique through a hole sand blasted at the side of the counter electrodes. Finally the holes were sealed and contacts were made for testing. For dummy cells, a similar fabrication procedure was followed expect the dye sensitization.

Photovoltaic Characterization. A 450 W xenon lamp (Oriel, USA) was used as light source for photovoltaic (*J*−*V*) measurements. The spectral output of the lamp was filtered using a Schott K113 Tempax sunlight filter (Präzisions Glas & Optik GmbH, Germany) to reduce the mismatch between the simulated and actual solar spectrum to less than 4%. The *J*−*V* characteristics of the cells were recorded with a Keithley model 2400 digital source meter (Keithley, USA). The photoactive area of 0.159 cm^2 was defined using a blackened metal mask. IPCE is measured using a homemade apparatus fitted with a Gemini monochromator and a Stanford lock-in amplifier. The monochromatic light is chopped at a frequency of 2 Hz, and it is superimposed on a 5mW/cm^2 white light bias. The electron recombination and transport in the mesoporous film were measured by transient photovoltage and photocurrent decay measurements, respectively. The white light was generated by an array of LEDs, while a pulsed red light (0.05 s square pulse width) was controlled by a fast solid-state switch to ascertain rapid sub-millisecond rise of light perturbation. The current and voltage decay were recorded on a Mac-interfaced Keithley 2602 source meter.

Conflict of Interest: The authors declare no competing financial interest.

Acknowledgment. The authors acknowledge the financial contribution from EU FP7 project "ORION" (grant agreement no. NMP-229036) and MOLESOL (FP7-Energy-2010-FET project contract no. 256617). The authors are grateful for the financial support from the Balzan Foundation as a part of the 2009 Balzan Prize awarded to M.G.

Supporting Information Available: XRD pattern of different thicknesses of ZnO on alumina templates, absorption spectra and IPCE of Y123 on different thicknesses of ZnO and TiO_2, absorption spectra of Y123 on acidic np-TiO_2, basic np-TiO_2, and np-Al_2O_3, DOS distribution below the conduction band, and diffusion coefficient of electrons in zinc oxide and titanium dioxide are provided. This material is available free of charge *via* the Internet at http://pubs.acs.org.

REFERENCES AND NOTES

1. Gratzel, M. Photoelectrochemical Cells. *Nature* **2001**, *414*, 338–344.
2. Hagfeldt, A.; Boschloo, G.; Sun, L.; Kloo, L.; Pettersson, H. Dye-Sensitized Solar Cells. *Chem. Rev.* **2010**, *110*, 6595–6663.
3. Listorti, A.; O'Regan, B.; Durrant, J. R. Electron Transfer Dynamics in Dye-Sensitized Solar Cells. *Chem. Mater.* **2011**, *23*, 3381–3399.
4. Yella, A.; Lee, H.-W.; Tsao, H. N.; Yi, C.; Chandiran, A. K.; Nazeeruddin, M. K.; Diau, E. W.-G.; Yeh, C.-Y.; Zakeeruddin, S. M.; Grätzel, M. Porphyrin-Sensitized Solar Cells with Cobalt (II/III)-Based Redox Electrolyte Exceed 12% Efficiency. *Science* **2011**, *334*, 629–634.
5. Grätzel, M. Solar Energy Conversion by Dye-Sensitized Photovoltaic Cells. *Inorg. Chem.* **2005**, *44*, 6841–6851.
6. Ito, S.; Murakami, T. N.; Comte, P.; Liska, P.; Grätzel, C.; Nazeeruddin, M. K.; Grätzel, M. Fabrication of Thin Film Dye Sensitized Solar Cells with Solar to Electric Power Conversion Efficiency over 10%. *Thin Solid Films* **2008**, *516*, 4613–4619.
7. Peter, L. M. Dye-Sensitized Nanocrystalline Solar Cells. *Phys. Chem. Chem. Phys.* **2007**, *9*, 2630–2642.
8. O'Regan, B. C.; Durrant, J. R. Kinetic and Energetic Paradigms for Dye-Sensitized Solar Cells: Moving from the Ideal to the Real. *Acc. Chem. Res.* **2009**, *42*, 1799–1808.
9. Kay, A.; Grätzel, M. Dye-Sensitized Core—Shell Nanocrystals: Improved Efficiency of Mesoporous Tin Oxide Electrodes Coated with a Thin Layer of an Insulating Oxide. *Chem. Mater.* **2002**, *14*, 2930–2935.
10. Chandiran, A. K.; Sauvage, F.; Casas-Cabanas, M.; Comte, P.; Zakeeruddin, S. M.; Graetzel, M. Doping a TiO_2 Photoanode with Nb^{5+} to Enhance Transparency and Charge Collection Efficiency in Dye-Sensitized Solar Cells. *J. Phys. Chem. C* **2010**, *114*, 15849–15856.
11. Chandiran, A. K.; Comte, P.; Humphry-Baker, R.; Kessler, F.; Yi, C.; Nazeeruddin, M. K.; Grätzel, M. Evaluating the Critical Thickness of TiO_2 Layer on Insulating Mesoporous Templates for Efficient Current Collection in Dye-Sensitized Solar Cells. *Adv. Funct. Mater.* **2013**, *23*, 2775–2781.
12. Mor, G. K.; Shankar, K.; Paulose, M.; Varghese, O. K.; Grimes, C. A. Use of Highly-Ordered TiO_2 Nanotube Arrays in Dye-Sensitized Solar Cells. *Nano Lett.* **2005**, *6*, 215–218.
13. Quintana, M.; Edvinsson, T.; Hagfeldt, A.; Boschloo, G. Comparison of Dye-Sensitized ZnO and TiO_2 Solar Cells: Studies of Charge Transport and Carrier Lifetime. *J. Phys. Chem. C* **2006**, *111*, 1035–1041.
14. Barea, E.; Xu, X.; Gonzalez-Pedro, V.; Ripolles-Sanchis, T.; Fabregat-Santiago, F.; Bisquert, J. Origin of Efficiency Enhancement in Nb_2O_5 Coated Titanium Dioxide Nanorod Based Dye Sensitized Solar Cells. *Energy Environ. Sci.* **2011**, *4*, 3414–3419.
15. Kim, H.-N.; Moon, J. H. Enhanced Photovoltaic Properties of Nb_2O_5-Coated TiO_2 3D Ordered Porous Electrodes in Dye-Sensitized Solar Cells. *ACS Appl. Mater. Interfaces* **2012**, *4*, 5821–5825.
16. Fan, J.; Hao, Y.; Cabot, A.; Johansson, E. M. J.; Boschloo, G.; Hagfeldt, A. Cobalt(II/III) Redox Electrolyte in ZnO Nanowire-Based Dye-Sensitized Solar Cells. *ACS Appl. Mater. Interfaces* **2013**, *5*, 1902–1906.
17. Willis, R. L.; Olson, C.; O'Regan, B.; Lutz, T.; Nelson, J.; Durrant, J. R. Electron Dynamics in Nanocrystalline ZnO and TiO_2 Films Probed by Potential Step Chronoamperometry and Transient Absorption Spectroscopy. *J. Phys. Chem. B* **2002**, *106*, 7605–7613.
18. Keis, K.; Lindgren, J.; Lindquist, S.-E.; Hagfeldt, A. Studies of the Adsorption Process of Ru Complexes in Nanoporous ZnO Electrodes. *Langmuir* **2000**, *16*, 4688–4694.
19. Liu, B.; Zeng, H. C. Hydrothermal Synthesis of ZnO Nanorods in the Diameter Regime of 50 nm. *J. Am. Chem. Soc.* **2003**, *125*, 4430–4431.
20. Bauer, C.; Boschloo, G.; Mukhtar, E.; Hagfeldt, A. Electron Injection and Recombination in $Ru(dcbpy)_2(NCS)_2$ Sensitized Nanostructured ZnO. *J. Phys. Chem. B* **2001**, *105*, 5585–5588.
21. Tiwana, P.; Docampo, P.; Johnston, M. B.; Snaith, H. J.; Herz, L. M. Electron Mobility and Injection Dynamics in Mesoporous ZnO, SnO_2, and TiO_2 Films Used in Dye-Sensitized Solar Cells. *ACS Nano* **2011**, *5*, 5158–5166.
22. Jiang, C. Y.; Sun, X. W.; Lo, G. Q.; Kwong, D. L.; Wang, J. X. Improved Dye-Sensitized Solar Cells with a ZnO-Nanoflower Photoanode. *Appl. Phys. Lett.* **2007**, *90*, 263501.
23. Zhang, Q.; Dandeneau, C. S.; Zhou, X.; Cao, G. ZnO Nanostructures for Dye-Sensitized Solar Cells. *Adv. Mater.* **2009**, *21*, 4087–4108.
24. Westermark, K.; Rensmo, H.; Siegbahn, H.; Keis, K.; Hagfeldt, A.; Ojamäe, L.; Persson, P. PES Studies of $Ru(dcbpyH_2)_2(NCS)_2$ Adsorption on Nanostructured ZnO for Solar Cell Applications. *J. Phys. Chem. B* **2002**, *106*, 10102–10107.
25. Schölin, R.; Quintana, M.; Johansson, E. M. J.; Hahlin, M.; Marinado, T.; Hagfeldt, A.; Rensmo, H. Preventing Dye Aggregation on ZnO by Adding Water in the Dye-Sensitization Process. *J. Phys. Chem. C* **2011**, *115*, 19274–19279.
26. Zhang, Q.; Chou, T. P.; Russo, B.; Jenekhe, S. A.; Cao, G. Aggregation of ZnO Nanocrystallites for High Conversion Efficiency in Dye-Sensitized Solar Cells. *Angew. Chem.* **2008**, *120*, 2436–2440.
27. Shi, Y.; Zhu, C.; Wang, L.; Zhao, C.; Li, W.; Fung, K. K.; Ma, T.; Hagfeldt, A.; Wang, N. Ultrarapid Sonochemical Synthesis of ZnO Hierarchical Structures: From Fundamental Research to High Efficiencies up to 6.42% for Quasi-Solid Dye-Sensitized Solar Cells. *Chem. Mater.* **2013**, *25*, 1000–1012.
28. Martinson, A. B. F.; Elam, J. W.; Hupp, J. T.; Pellin, M. J. ZnO Nanotube Based Dye-Sensitized Solar Cells. *Nano Lett.* **2007**, *7*, 2183–2187.
29. Rensmo, H.; Keis, K.; Lindström, H.; Södergren, S.; Solbrand, A.; Hagfeldt, A.; Lindquist, S.-E.; Wang, L. N.; Muhammed, M. High Light-to-Energy Conversion Efficiencies for Solar Cells Based on Nanostructured ZnO Electrodes. *J. Phys. Chem. B* **1997**, *101*, 2598–2601.
30. Law, M.; Greene, L. E.; Johnson, J. C.; Saykally, R.; Yang, P. Nanowire Dye-Sensitized Solar Cells. *Nat. Mater.* **2005**, *4*, 455–459.
31. Baxter, J. B.; Aydil, E. S. Nanowire-Based Dye-Sensitized Solar Cells. *Appl. Phys. Lett.* **2005**, *86*, 53114.
32. Ferrere, S.; Zaban, A.; Gregg, B. A. Dye Sensitization of Nanocrystalline Tin Oxide by Perylene Derivatives. *J. Phys. Chem. B* **1997**, *101*, 4490–4493.
33. Snaith, H. J.; Ducati, C. SnO_2-Based Dye-Sensitized Hybrid Solar Cells Exhibiting Near Unity Absorbed Photon-to-Electron Conversion Efficiency. *Nano Lett.* **2010**, *10*, 1259–1265.
34. Gomes, M. A. B.; Bulhões, L. O. de S.; de Castro, S. C.; Damião, A. J. The Electrochromic Process at Nb_2O_5 Electrodes Prepared by Thermal Oxidation of Niobium. *J. Electrochem. Soc.* **1990**, *137*, 3067–3070.
35. Chen, S. G.; Chappel, S.; Diamant, Y.; Zaban, A. Preparation of Nb_2O_5 Coated TiO_2 Nanoporous Electrodes and Their Application in Dye-Sensitized Solar Cells. *Chem. Mater.* **2001**, *13*, 4629–4634.
36. Le Viet, A.; Jose, R.; Reddy, M. V; Chowdari, B. V. R.; Ramakrishna, S. Nb_2O_5 Photoelectrodes for Dye-Sensitized Solar Cells: Choice of the Polymorph. *J. Phys. Chem. C* **2010**, *114*, 21795–21800.
37. Ghosh, R.; Brennaman, M. K.; Uher, T.; Ok, M.-R.; Samulski, E. T.; McNeil, L. E.; Meyer, T. J.; Lopez, R. Nanoforest Nb_2O_5 Photoanodes for Dye-Sensitized Solar Cells by Pulsed Laser Deposition. *ACS Appl. Mater. Interfaces* **2011**, *3*, 3929–3935.

38. Sayama, K.; Sugihara, H.; Arakawa, H. Photoelectrochemical Properties of a Porous Nb_2O_5 Electrode Sensitized by a Ruthenium Dye. *Chem. Mater.* **1998**, *10*, 3825–3832.
39. Ou, J. Z.; Rani, R. A.; Ham, M.-H.; Field, M. R.; Zhang, Y.; Zheng, H.; Reece, P.; Zhuiykov, S.; Sriram, S.; Bhaskaran, M.; *et al*. Elevated Temperature Anodized Nb_2O_5: A Photoanode Material with Exceptionally Large Photoconversion Efficiencies. *ACS Nano* **2012**, *6*, 4045–4053.
40. Burnside, S.; Moser, J.-E.; Brooks, K.; Grätzel, M.; Cahen, D. Nanocrystalline Mesoporous Strontium Titanate as Photoelectrode Material for Photosensitized Solar Devices: Increasing Photovoltage through Flatband Potential Engineering. *J. Phys. Chem. B* **1999**, *103*, 9328–9332.
41. Dabestani, R.; Bard, A. J.; Campion, A.; Fox, M. A.; Mallouk, T. E.; Webber, S. E.; White, J. M. Sensitization of Titanium Dioxide and Strontium Titanate Electrodes by Ruthenium(II) Tris(2,2′-Bipyridine-4,4′-Dicarboxylic Acid) and Zinc Tetrakis(4-Carboxyphenyl)porphyrin: An Evaluation of Sensitization Efficiency for Component Photoelectrodes in a Mul. *J. Phys. Chem.* **1988**, *92*, 1872–1878.
42. Yang, S.; Kou, H.; Wang, J.; Xue, H.; Han, H. Tunability of the Band Energetics of Nanostructured $SrTiO_3$ Electrodes for Dye-Sensitized Solar Cells. *J. Phys. Chem. C* **2010**, *114*, 4245–4249.
43. Shin, S. S.; Kim, J. S.; Suk, J. H.; Lee, K. D.; Kim, D. W.; Park, J. H.; Cho, I. S.; Hong, K. S.; Kim, J. Y. Improved Quantum Efficiency of Highly Efficient Perovskite $BaSnO_3$-Based Dye-Sensitized Solar Cells. *ACS Nano* **2013**, *7*, 1027–1035.
44. Tan, B.; Toman, E.; Li, Y.; Wu, Y. Zinc Stannate (Zn_2SnO_4) Dye-Sensitized Solar Cells. *J. Am. Chem. Soc.* **2007**, *129*, 4162–4163.
45. Ozgur, U.; Alivov, Y. I.; Liu, C.; Teke, A.; Reshchikov, M. A.; Dogan, S.; Avrutin, V.; Cho, S.-J.; Morkoc, H. A Comprehensive Review of ZnO Materials and Devices. *J. Appl. Phys.* **2005**, *98*, 41301.
46. Tang, H.; Prasad, K.; Sanjines, R.; Schmid, P. E.; Levy, F. Electrical and Optical Properties of TiO_2 Anatase Thin Films. *J. Appl. Phys.* **1994**, *75*, 2042–2047.
47. Bae, H. S.; Yoon, M. H.; Kim, J. H.; Im, S. Photodetecting Properties of ZnO-Based Thin-Film Transistors. *Appl. Phys. Lett.* **2003**, *83*, 5313–5315.
48. Nelson, J. J.; Amick, T. J.; Elliott, C. M. Mass Transport of Polypyridyl Cobalt Complexes in Dye-Sensitized Solar Cells with Mesoporous TiO_2 Photoanodes. *J. Phys. Chem. C* **2008**, *112*, 18255–18263.
49. Feldt, S. M.; Gibson, E. A.; Gabrielsson, E.; Sun, L.; Boschloo, G.; Hagfeldt, A. Design of Organic Dyes and Cobalt Polypyridine Redox Mediators for High-Efficiency Dye-Sensitized Solar Cells. *J. Am. Chem. Soc.* **2010**, *132*, 16714–16724.
50. Chandiran, A. K.; Yella, A.; Stefik, M.; Heiniger, L.-P.; Comte, P.; Nazeeruddin, M. K.; Grätzel, M. Low-Temperature Crystalline Titanium Dioxide by Atomic Layer Deposition for Dye-Sensitized Solar Cells. *ACS Appl. Mater. Interfaces* **2013**, *5*, 3487–3493.
51. Katz, M. J.; Vermeer, M. J. D.; Farha, O. K.; Pellin, M. J.; Hupp, J. T. Effects of Adsorbed Pyridine Derivatives and Ultrathin Atomic-Layer-Deposited Alumina Coatings on the Conduction Band-Edge Energy of TiO_2 and on Redox-Shuttle-Derived Dark Currents. *Langmuir* **2012**, *29*, 806–814.
52. George, S. M. Atomic Layer Deposition: An Overview. *Chem. Rev.* **2009**, *110*, 111–131.
53. Leskelä, M.; Ritala, M. Atomic Layer Deposition (ALD): From Precursors to Thin Film Structures. *Thin Solid Films* **2002**, *409*, 138–146.
54. Elam, J. W.; Routkevitch, D.; Mardilovich, P. P.; George, S. M. Conformal Coating on Ultrahigh-Aspect-Ratio Nanopores of Anodic Alumina by Atomic Layer Deposition. *Chem. Mater.* **2003**, *15*, 3507–3517.
55. Tsao, H. N.; Comte, P.; Yi, C.; Grätzel, M. Avoiding Diffusion Limitations in Cobalt(III/II)-Tris(2,2′-Bipyridine)-Based Dye-Sensitized Solar Cells by Tuning the Mesoporous TiO_2 Film Properties. *ChemPhysChem* **2012**, *13*, 2976–2981.
56. Xu, Y.; Schoonen, M. The Absolute Energy Positions of Conduction and Valence Bands of Selected Semiconducting Minerals. *Am. Mineral.* **2000**, *85*, 543–556.
57. Barnes, P. R. F.; Anderson, A. Y.; Koops, S. E.; Durrant, J. R.; O'Regan, B. C. Electron Injection Efficiency and Diffusion Length in Dye-Sensitized Solar Cells Derived from Incident Photon Conversion Efficiency Measurements. *J. Phys. Chem. C* **2008**, *113*, 1126–1136.
58. Koops, S. E.; O'Regan, B. C.; Barnes, P. R. F.; Durrant, J. R. Parameters Influencing the Efficiency of Electron Injection in Dye-Sensitized Solar Cells. *J. Am. Chem. Soc.* **2009**, *131*, 4808–4818.
59. Bahnemann, D. W.; Kormann, C.; Hoffmann, M. R. Preparation and Characterization of Quantum Size Zinc Oxide: A Detailed Spectroscopic Study. *J. Phys. Chem.* **1987**, *91*, 3789–3798.
60. Chandiran, A. K.; Tetreault, N.; Humphry-Baker, R.; Kessler, F.; Baranoff, E.; Yi, C.; Nazeeruddin, M. K.; Grätzel, M. Subnanometer Ga_2O_3 Tunnelling Layer by Atomic Layer Deposition to Achieve 1.1 V Open-Circuit Potential in Dye-Sensitized Solar Cells. *Nano Lett.* **2012**, *12*, 3941–3947.
61. Kormann, C.; Bahnemann, D. W.; Hoffmann, M. R. Preparation and Characterization of Quantum-Size Titanium Dioxide. *J. Phys. Chem.* **1988**, *92*, 5196–5201.
62. Li, T. C.; Góes, M. S.; Fabregat-Santiago, F.; Bisquert, J.; Bueno, P. R.; Prasittichai, C.; Hupp, J. T.; Marks, T. J. Surface Passivation of Nanoporous TiO_2 *via* Atomic Layer Deposition of ZrO_2 for Solid-State Dye-Sensitized Solar Cell Applications. *J. Phys. Chem. C* **2009**, *113*, 18385–18390.
63. Son, H.-J.; Wang, X.; Prasittichai, C.; Jeong, N. C.; Aaltonen, T.; Gordon, R. G.; Hupp, J. T. Glass-Encapsulated Light Harvesters: More Efficient Dye-Sensitized Solar Cells by Deposition of Self-Aligned, Conformal, and Self-Limited Silica Layers. *J. Am. Chem. Soc.* **2012**, *134*, 9537–9540.
64. Pourret, A.; Guyot-Sionnest, P.; Elam, J. W. Atomic Layer Deposition of ZnO in Quantum Dot Thin Films. *Adv. Mater.* **2009**, *21*, 232–235.
65. Xie, Q.; Jiang, Y.-L.; Detavernier, C.; Deduytsche, D.; Van Meirhaeghe, R. L.; Ru, G.-P.; Li, B.-Z.; Qu, X.-P. Atomic Layer Deposition of TiO_2 from Tetrakis-Dimethyl-Amido Titanium or Ti Isopropoxide Precursors and H_2O. *J. Appl. Phys.* **2007**, *102*, 83521.
66. Musschoot, J.; Xie, Q.; Deduytsche, D.; Van den Berghe, S.; Van Meirhaeghe, R. L.; Detavernier, C. Atomic Layer Deposition of Titanium Nitride from TDMAT Precursor. *Microelectron. Eng.* **2009**, *86*, 72–77.
67. Tsao, H. N.; Yi, C.; Moehl, T.; Yum, J.-H.; Zakeeruddin, S. M.; Nazeeruddin, M. K.; Grätzel, M. Cyclopentadithiophene Bridged Donor−Acceptor Dyes Achieve High Power Conversion Efficiencies in Dye-Sensitized Solar Cells Based on the Tris-Cobalt Bipyridine Redox Couple. *ChemSusChem* **2011**, *4*, 591–594.